China Ocean Eng., 2020, Vol. 34, No. 6, P. 784–794
DOI: https://doi.org/10.1007/s13344-020-0071-z, ISSN 0890-5487
http://www.chinaoceanengin.cn/ E-mail: coe@nhri.cn

Penetration Resistance of Skirt-Tip with Rough Base for Suction Caissons in Clay

WU Yu-qi[a], LI Da-yong[b, c, *], YANG Qing[a]

[a] State Key Laboratory of Coastal and Offshore Engineering, Dalian University of Technology, Dalian 116024, China

[b] College of Civil Engineering, Fuzhou University, Fuzhou 350108, China

[c] College of Civil Engineering and Architecture, Shandong University of Science and Technology, Qingdao 266590, China

Received January 10, 2020; revised July 22, 2020; accepted August 20, 2020

Abstract

Suction caissons can readily penetrate into the seabed under the combination of the self-weight and suction resulted from the encased water being increasingly pumped out. During suction-assisted penetration, the equivalent overburden at the skirt-tip level outside the caisson is generally higher than that inside because the vertical stress within the soil plug is reduced by the exerted suction. This may result in a uniform shear stress developing over the base of the skirt-tip as the soil below the skirt-tip tends to move into the caisson, which leads to an asymmetric failure wedge existing below the base of the skirt-tip. Besides, different adhesion factors along the inside (α_i) and outside (α_o) of the skirt wall will cause asymmetric plastic zones inside and outside the caisson. Accordingly, an asymmetric failure mechanism is therefore proposed to calculate the penetration resistance of the skirt-tip. The proposed failure mechanism is the first to consider the effect of different adhesion factors (α_i) and (α_o) on the failure mechanism at the skirt-tip, and involves the contribution from the weighted average of equivalent overburdens inside and outside caisson at the skirt-tip level. The required suction pressure can be obtained in terms of force equilibrium of the caisson in a vertical direction. Finally, the asymmetric failure mechanism at the skirt-tip is validated with the FE calculations. By comparing with the measured data, the predictions of the required suction pressure are found to be in good agreement with the experimental results.

Key words: suction caisson, required suction pressure, penetration resistance, skirt-tip, rough base, clay

Citation: Wu, Y. Q., Li, D. Y., Yang, Q., 2020. Penetration resistance of skirt-tip with rough base for suction caissons in clay. China Ocean Eng., 34(6): 784–794, doi: https://doi.org/10.1007/s13344-020-0071-z

1 Introduction

Suction caissons have become the preferred foundation for offshore wind turbines due to their competitive technical and economic advantages over other foundations like driven piles (Zhang et al., 2016; Wu et al., 2019; Luan et al., 2020). A suction caisson is first penetrated into the seabed to a certain depth under its self-weight, and further penetration is achieved by pumping out the encased water, creating an under-pressure inside the caisson. During installation, the total penetration resistance (F_{tot}) is composed of the skirt-tip resistance (F_{tip}) and skin frictions along the inside (F_i) and outside (F_o) of the skirt wall. The skin frictions can be calculated by applying an adhesion factor α to the value of in-situ undrained shear strength s_u (Houlsby and Byrne, 2005; Westgate et al., 2009), where the adhesion factor equals the inverse of the sensitivity S_t (Andersen and Jostad, 1999; Houlsby and Byrne, 2005). The skirt-tip resistance can be computed from $F_{tip}=\pi D_m t\sigma_{tip}=\pi D_m t(N_q\sigma_z+N_c s_u)$, where, N_q and N_c are the bearing capacity factors; D_m is the mean diameter of caisson; t is the thickness of skirt wall; σ_z is the weighted average of equivalent overburdens at depth z (Chen and Randolph, 2004; Houlsby and Byrne, 2005; Li et al., 2010; Randolph et al., 2005; Westgate et al., 2009). Since the caisson penetration is faster than the drainage of clay, the shear strength of clay can be regarded as undrained strength. For the undrained clay, it has the bearing capacity factor N_q=1. However, an appreciable difference exists in selecting the value of the bearing capacity factor N_c among some researchers. Andersen et al. (2005) recommended that the factor N_c ranges from 7.5 to 11, the higher num-

Foundation item: This study was financially supported by the National Natural Science Foundation of China (Grant Nos. 51639002 and 51879044) and the SDUST Research Fund (Grant No. 2015KYJH104).

*Corresponding author. E-mail: ldy@fzu.edu.cn

ber considered the influence of the skin friction above the bearing area. Reductions in factor N_c were made for depth effects in the cases of shallow penetration. Li et al. (2010) indicted that N_c increases from 6.2 at embedment depth h/D=0 to 9.0 at $h/D \geqslant 4$. Furthermore, slightly overestimated values of N_c were obtained by Zhou and Randolph (2006), which reduces from 11.6 at 1.0D embedment depth to 9.2 at 4.0D embedment depth. Westgate et al. (2009) pointed out that the factor N_c could be as small as 6.2 and as large as 15, resulting in a significant uncertainty in the calculation of penetration resistance (Hossain et al., 2012). In addition, N_c=7.5 (Watson et al., 2000; Randolph and House, 2002; Randolph et al., 2005; Andersen and Jostad, 1999; Chen and Randolph, 2004; Hossain et al., 2012) and N_c=9.0 (Byrne et al., 2002; Guo et al., 2012; Houlsby and Byrne, 2005; Houlsby et al., 2005) were typically suggested to calculate the skirt-tip resistance. Obviously, there has been some uncertainty in the quantification of factor N_c (Watson et al., 2000), which will lead to inaccurate estimation of the skirt-tip resistance. Chen and Randolph (2004) pointed out that factor N_c varying from 7 to 12 will lead to a difference of 9% in total penetration resistance.

A slip-line method is adopted in this paper to derive an analytical solution to skirt-tip resistance with rough base according to the asymmetrical failure mechanism. The proposed failure mechanism will consider the effect of different adhesion factors α_i and α_o on the failure mechanism at the skirt-tip, and involves the contribution from both the effective unit weight of soil within plastic zones and the weighted average of equivalent overburdens at the skirt-tip level. Ultimately, the bearing capacity factors N_c and N_γ will be expressed in terms of adhesion factors α_i and α_o, and used to compute the required suction pressure based on the force equilibrium of the caisson in the vertical direction. By comparing with the finite element (FE) calculations, the asymmetry failure mechanism at the skirt-tip is validated. In addition, the experimental results were further analyzed by the proposed method to testify the rationality of the presented theoretical results.

2 Penetration resistance of skirt-tip with rough base

In the case of a surface foundation, a symmetrical failure mechanism with a plastic failure wedge below the foundation is often used for a smooth base (Meyerhof, 1951). For a rough base, a symmetrical elastic failure wedge is commonly considered to exist below the base of the foundation (Terzaghi, 1943; Meyerhof, 1951, 1955, 1963). The geometry of the failure wedge below the base of the foundation can be defined by the base angle ω that is usually assumed from the internal friction angle of soil φ (Terzaghi, 1943) to $\pi/4+\varphi/2$ (Meyerhof, 1951, 1963). However, in the case of suction caissons penetrating into clay under suction, the equivalent overburden at the skirt-tip level outside caisson (σ_o) is generally higher than that inside (σ_i) since the exerted suction inside the caisson reduces the vertical stress within the soil plug. As a result, the soil below the base of the skirt-tip tends to move inwards, leading to a uniform base shear stress (τ_{tip}) develops at the skirt-tip, rather than that increases linearly with the distance from the center line of skirt wall to a maximum at the end of the failure wedge (Meyerhof, 1955). The shear stress at the base of skirt-tip (τ_{tip}) will cause an asymmetric geometry of the failure wedge below the skirt-tip, as shown in Fig. 1.

As suggested by Meyerhof (1951), the zones of plastic equilibrium around the foundation extend towards the sides of the foundation with the increasing embedment depth. Since the skirt walls are generally very thin compared with the caisson diameter, D/t > 100, where D is the outer diameter of caisson (Randolph et al., 1998; House et al., 1999), the skirt wall tends to be a long slender element. Thus, the failure mechanism at the skirt-tip may resemble that of a deep foundation where the plastic zone has reached the sides of the skirt wall. Moreover, the various adhesion factors (α_i) and (α_o) will lead to different skin frictions, resulting in asymmetric plastic zones between the inside and outside of the caisson. Consequently, an asymmetrical failure mechanism may occur at the skirt-tip. Since the shear stresses along the inside and outside of the skirt wall are $\tau_i=\alpha_i s_u$ and $\tau_o=\alpha_o s_u$, respectively. For simplicity, it is assumed that the shear stress $\tau_{tip}=0.5(\alpha_i+\alpha_o)s_u$ distributes uniformly over the base of the skirt-tip. As shown in Fig. 1, an asymmetrical failure mechanism may be formed at the skirt-tip, where the geometry of failure wedge I can be defined by the base angles ω_i and ω_o. The plastic zones on each side of the asymmetrical failure wedge consist of radial shear zone II and plane shear zone III that are identical to those of the failure mechanism for a deep foundation as presented by Meyerhof (1951). Since the skirt walls are generally very thin compared with the caisson diameter, the displacement pattern of the clay within plastic zones at the skirt-tip may be very close to a plane strain problem (Andersen et al., 2008; Randolph et al., 2005; Wu et al., 2018, 2019). Then, under plain-strain condition, the limit equilibrium differen-

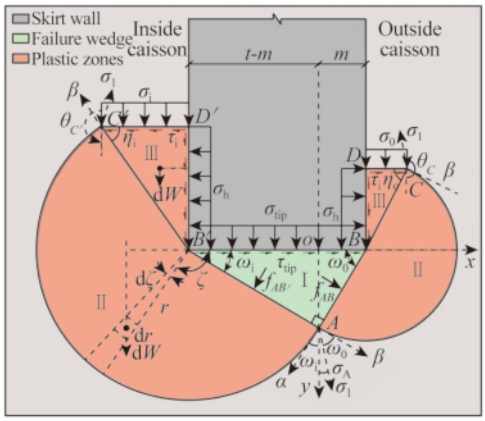

Fig. 1. Asymmetrical failure mechanism.

tial equations of the slip-line can be obtained in terms of the stress equilibrium and yield criterion. In deriving the slip-line solutions, the soils within zones I to III are assumed to be isotropic and ideally rigid-plastic materials with associated flow rule and their weight and volumetric deformation are ignored. As suggested by Davis and Booker (1973), it is accurate enough to use some average value of s_u as a constant in bearing capacity analysis for small footings in undrained clay (φ=0). Thus, it is assumed that the undrained shear strength within plastic zones at the skirt-tip is approximately uniform.

2.1 Failure wedge I

As suggested by Meyerhof (1951), the failure wedge ABB' acts as part of the skirt wall. Thus, boundaries AB and AB' shall be slip-lines that perpendicularly intersect with each other at point A, as shown in Fig. 1. Since the weight of soil within zone I is ignored, the shear and normal stresses on boundaries AB and AB' can be determined graphically by using Mohr's circle. Thus, as shown in Fig. 2b, the stress condition on boundary BB' can be represented by that at point o on a Mohr circle. Then, a chord from o, drawn parallel to the boundary BB' in the physical plane, intersects the Mohr circle at point a that is defined as the pole point (Li et al., 2013). On the Mohr circle, if two chords are drawn from point a to points b and b'. Then, ab and ab' will be parallel to slip-lines AB and AB' in the physical plane on which the shear strengths of soil develop fully.

Thus, from Fig. 2b, the geometry of the asymmetrical failure wedge ABB' is uniquely defined by the base angles ω_i and ω_o that can be derived in terms of the base shear stress τ_{tip} as:

$$\begin{cases} \omega_i = \dfrac{1}{2}\arccos\dfrac{\tau_{tip}}{s_u} = \dfrac{1}{2}\arccos\dfrac{(\alpha_i+\alpha_o)s_u}{2s_u} = \dfrac{1}{2}\arccos\dfrac{\alpha_i+\alpha_o}{2} \\ \omega_o = \dfrac{\pi}{4}+\dfrac{1}{2}\arcsin\dfrac{|\tau_{tip}|}{s_u} = \dfrac{\pi}{4}+\dfrac{1}{2}\arcsin\dfrac{(\alpha_i+\alpha_o)s_u}{2s_u} = \dfrac{\pi}{4}+ \\ \dfrac{1}{2}\arcsin\dfrac{\alpha_i+\alpha_o}{2} \end{cases} \tag{1}$$

From Fig. 2a, the direction of major principle stress σ_1 at point A can be expressed as:

$$\theta_A = \frac{\pi}{4}-\omega_i = \omega_o-\frac{\pi}{4}. \tag{2}$$

2.2 Stress fields in plastic zones

2.2.1 *Basic equations*

As shown in Fig. 3, the compressive stresses σ_x and σ_y are treated as positive. The shear stress τ_{xy} on a given plane is positive if τ_{xy} tends to produce a counterclockwise rotation about a point inside the soil element, and the shear stress τ_{xy} is negative if τ_{xy} tends to rotate clockwise about a point inside the element. From Fig. 3, we have the following two equations of equilibrium

$$\begin{cases} \dfrac{\partial\sigma_x}{\partial x}+\dfrac{\partial\tau_{xy}}{\partial y}=0 \\ \dfrac{\partial\tau_{xy}}{\partial x}+\dfrac{\partial\sigma_y}{\partial y}=0 \end{cases} \tag{3}$$

The yield condition of clay is shown in Fig. 4. Then, the stresses can be expressed as:

$$\begin{cases} \sigma_x = p-r\cos 2\theta \\ \sigma_y = p+r\cos 2\theta \\ \tau_{xy} = \pm r\sin 2\theta \end{cases} \tag{4}$$

where $p=(\sigma_x+\sigma_y)/2$ is the mean stress, $r=s_u$ is the radius of Mohr circle, θ is the angle between the direction of the major principle stress σ_1 and the y-axis.

By substituting Eq. (4) into Eq. (3), the following two equations which are known as the Hencky equations can be obtained

$$\begin{cases} p-2s_u\theta = C_\alpha \ \text{ along an } \alpha\text{−line} \\ p+2s_u\theta = C_\beta \ \text{ along a } \beta\text{−line} \end{cases} \tag{5}$$

where C_α and C_β are constants along α and β slip-lines.

From Fig. 1, points A and C', A and C are on the same α and β slip-lines, respectively. Thus, from Eq. (5), it has

$$\begin{cases} p_A-2s_u\theta_A = p_{C'}-2s_u\theta_{C'} \ \text{ along an } \alpha\text{−line} \\ p_A+2s_u\theta_A = p_C+2s_u\theta_C \ \text{ along a } \beta\text{−line} \end{cases} \tag{6}$$

where, p_A, p_C and $p_{C'}$ are the mean stresses at points A, C and C'; θ_A, θ_C and $\theta_{C'}$ are the angles between the major principle stresses σ_1 and y axis at points A, C and C', respect-

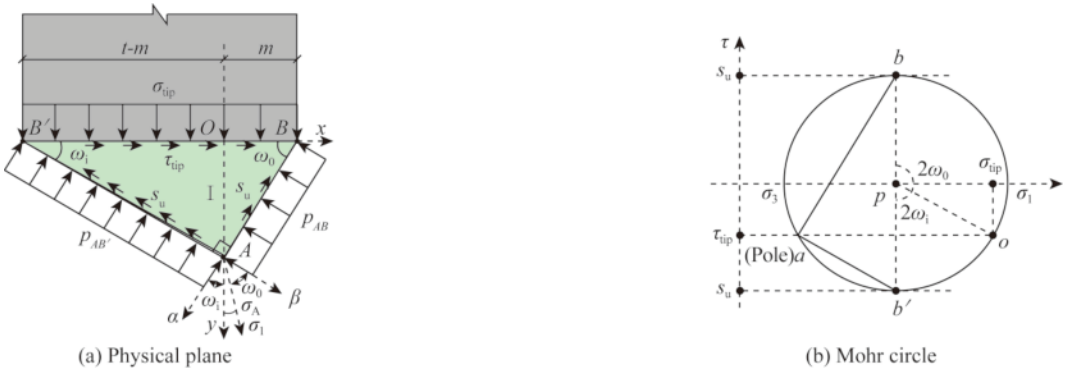

(a) Physical plane (b) Mohr circle

Fig. 2. Stress state of elastic wedge.

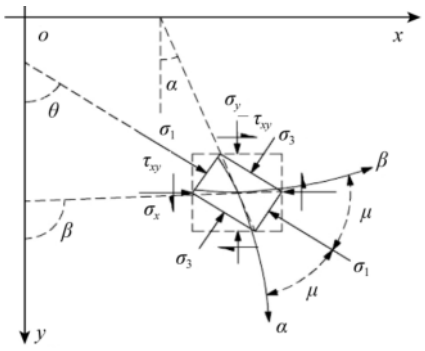

Fig. 3. Coordinate system and stress characteristic lines.

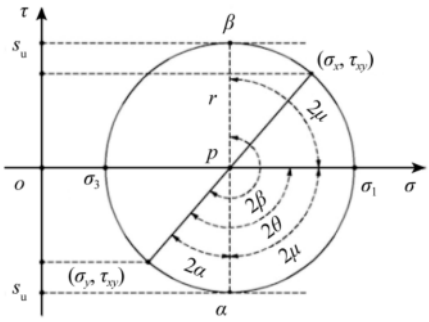

Fig. 4. Yield condition.

ively.

2.2.2 *Stress boundary conditions analysis*

As shown in Fig. 5, in the plastic zone, considering a boundary Γ whose normal stress forms an angle of ε with the y-axis, the normal and shear stress are known as σ_n and τ_n.

From Fig. 4, it has

$$\begin{cases} 2\mu = \pm\pi/2 \\ \alpha = \theta - \mu \\ \beta = \theta + \mu \end{cases} \tag{7}$$

On boundary Γ, the soil has reached the critical condition. According to Fig. 6, we can obtain

$$\begin{cases} \sigma_n = p + s_u \cos 2(\theta - \varepsilon) \\ \tau_n = s_u \sin 2(\theta - \varepsilon) \end{cases} \tag{8}$$

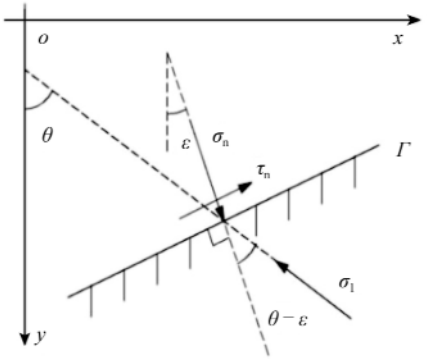

Fig. 5. Stress boundary condition.

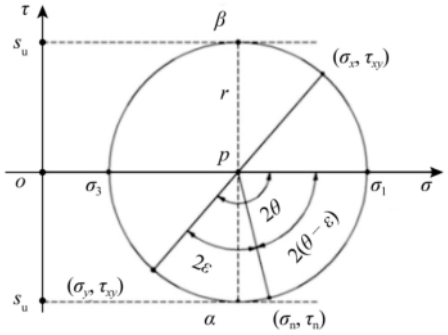

Fig. 6. Stress states at failure on boundary Γ.

From Eq. (8), p and θ can be solved in terms of the given values of σ_n, τ_n and ε, it has

$$\begin{cases} p = \sigma_n - s_u \cos 2(\theta - \varepsilon) \\ \theta = \varepsilon + \dfrac{1}{2}\arcsin\left(\dfrac{\tau_n}{s_u}\right) \end{cases} \tag{9}$$

2.2.3 *Construction of slip-line fields*

(1) Plane shear zone III inside the caisson

As discussed previously, the plastic zones inside the caisson have extended to the skirt wall. Thus, the shear strength of soil within plane shear zone III developed fully. Since the weight of the soil within plastic zones is ignored, the stress condition (σ_i, τ_i) on boundary $C'D'$ can be represented by point d' on a Mohr circle, as shown in Fig. 7b. Then, a chord from d' drawn parallel to boundary $D'C'$ in the physical plane, intersects the Mohr circle at point c' that is defined as the pole point (Li et al., 2013). On the Mohr circle, if a chord is drawn from pole point c' to point b', then chord $b'c'$ will be parallel to slip-line $B'C'$ in the physical plane.

From Fig. 7b, the inclination angle η_i of boundary $B'C'$ can be derived as:

$$\eta_i = \frac{1}{2}\left(\frac{\pi}{2} + \arcsin\frac{\tau_i}{s_u}\right) = \frac{1}{2}\left(\frac{\pi}{2} + \arcsin\frac{\alpha_i s_u}{s_u}\right) = \frac{\pi}{4} + \frac{1}{2}\arcsin\alpha_i. \tag{10}$$

From Fig. 7b, the mean stress $p_{C'}$ and the angle $\theta_{C'}$ at point C' can be obtained as:

$$\begin{cases} p_{C'} = \sigma_i + s_u \cos\left(2\eta_i - \dfrac{\pi}{2}\right) = \sigma_i + s_u\sqrt{1-\alpha_i^2} \\ \theta_{C'} = -\left(\dfrac{3\pi}{4} + \eta_i\right) = -\pi - \dfrac{1}{2}\arcsin\alpha_i \end{cases} \tag{11}$$

(2) Plane shear zone III outside the caisson

Similarly, from Fig. 8b, the inclination angle η_o of boundary BC can be derived as:

$$\eta_o = \frac{1}{2}\left(\frac{\pi}{2} + \arcsin\frac{\tau_o}{s_u}\right) = \frac{1}{2}\left(\frac{\pi}{2} + \arcsin\frac{\alpha_o s_u}{s_u}\right) = \frac{\pi}{4} + \frac{1}{2}\arcsin\alpha_o. \tag{12}$$

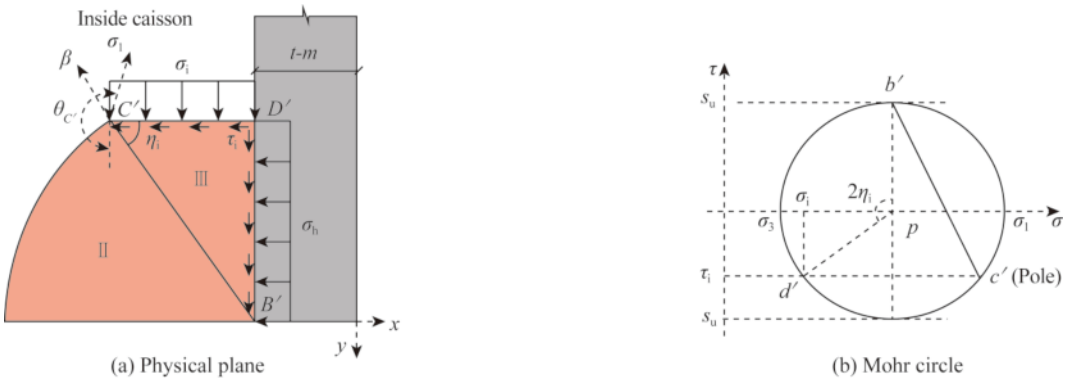

Fig. 7. Failure mechanism inside caisson.

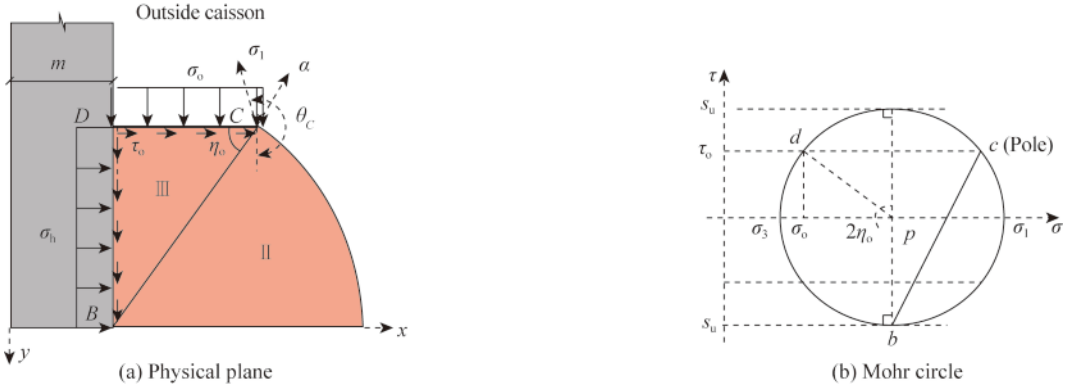

Fig. 8. Failure mechanism inside the caisson.

The mean stress p_C and the angle θ_C at point C can be expressed as:

$$\begin{cases} p_C = \sigma_o + s_u \cos\left(2\eta_o - \dfrac{\pi}{2}\right) = \sigma_o + s_u\sqrt{1-\alpha_o^2} \\ \theta_C = \dfrac{3\pi}{4} + \eta_o = \pi + \dfrac{1}{2}\arcsin\alpha_o \end{cases} \tag{13}$$

2.2.4 *Bearing capacity factors N_q and N_c*

According to the properties of the slip-line fields, if the slip-line fields on both sides are known, then the slip-line field between them can be determined uniquely. As shown in Fig. 1, since the one family of slip-lines are straight lines (e.g. AB, BC, AB' and $B'C'$) that meet at points B and B', respectively. Thus, in zone II, those of the other family should be circle arcs. By combining Eqs. (1), (2), (6), (11) and (13), the mean stress on boundaries AB' and AB can be respectively derived as:

$$\begin{cases} p_{AB'} = \sigma_i + s_u\left(2\pi + \arcsin\alpha_i + \arcsin\dfrac{\alpha_i+\alpha_o}{2} + \sqrt{1-\alpha_i^2}\right) \\ p_{AB} = \sigma_o + s_u\left(2\pi + \arcsin\alpha_o - \arcsin\dfrac{\alpha_i+\alpha_o}{2} + \sqrt{1-\alpha_o^2}\right) \end{cases} \tag{14}$$

From Fig. 2, based on the force equilibrium of failure wedge I, it is therefore essential to use the following expression to obtain the bearing capacity of the skirt-tip, F_{tip}

$$F_{tip} = p_{AB'}\frac{t-m}{\cos\omega_i}\cos\omega_i + s_u\frac{t-m}{\cos\omega_i}\sin\omega_i + p_{AB}\frac{m}{\cos\omega_o}\cos\omega_o + s_u\frac{m}{\cos\omega_o}\sin\omega_o, \tag{15}$$

where, $m=t(\tan\omega_i)/(\tan\omega_i+\tan\omega_o)$.

By substituting Eq. (14) into Eq. (15), in terms of weighted contributions from equivalent overburdens (σ_i) and (σ_o) and the undrained shear strength (s_u), the penetration resistance at the skit-tip σ_{tip} can be presented in a standard form as:

$$\sigma_{tip} = \frac{F_{tip}}{t} = \frac{p_{AB'}(t-m) + s_u(t-m)\tan\omega_i + p_{AB}m + s_u m\tan\omega_o}{t} =$$
$$\underbrace{\frac{\sigma_i\tan\omega_o + \sigma_o\tan\omega_i}{\tan\omega_i+\tan\omega_o}}_{N_q\sigma_z} + \underbrace{\left[\begin{array}{l} 2\pi + \arcsin\alpha_i + \arcsin\dfrac{\alpha_i+\alpha_o}{2} + \sqrt{1-\alpha_i^2} + 2\dfrac{\tan\omega_i\tan\omega_o}{\tan\omega_i+\tan\omega_o} \\ +\left(\arcsin\alpha_o - \arcsin\alpha_i + \sqrt{1-\alpha_o^2} - \sqrt{1-\alpha_i^2} - 2\arcsin\dfrac{\alpha_i+\alpha_o}{2}\right)\dfrac{\tan\omega_i}{\tan\omega_i+\tan\omega_o} \end{array}\right]}_{N_c s_u} s_u \tag{16}$$

where $\sigma_z=(\sigma_i\tan\omega_o+\sigma_o\tan\omega_i)/(\tan\omega_o+\tan\omega_i)$ is the weighted average of equivalent overburdens at the skirt-tip level in-

side and outside the caisson, ω_i and ω_o can be determined from Eq. (1). The first term of Eq. (16) is resulted from the weighted average of overburdens at the skirt-tip level σ_z, and the corresponding bearing capacity factor N_q=1. The second term of Eq. (16) arises from the undrained shear strength of soil s_u, and the corresponding factor N_c has the value as given in the square brackets of Eq. (16). Fig. 9a shows the values of factor N_c versus adhesion factors, which ranges from 8.28 to 9.42 with respect to variations of the adhesion factors α_i and α_o.

2.2.5 *Bearing capacity factor N_γ*

For the proposed asymmetry failure mechanism, the effective unit weight of clay within the plastic zones will contribute to the penetration resistance of skirt-tip. Thus, by considering the failure mechanism inside the caisson as shown in Fig. 1, the plastic equilibrium can be found by balancing the moments about point B' due to the self-weights of plain shear zone III, radio shear zone II and the overturning resultant thrust $f_{AB'}$ acting on boundary AB'.

The moment induced by the self-weight of plain shear zone III can be obtained as:

$$M_{III}=\frac{\gamma'(t-m)^3}{6\cos^3\omega_i}\sin\eta_i\cos^2\eta_i. \tag{17}$$

The moment caused by the self-weight of radio shear zone II can be calculated as:

$$M_{II}=\int_{\omega_i}^{\pi+\eta_i}\int_{0}^{\frac{t-m}{\cos\omega_i}} r^2\cos\xi\,\mathrm{d}r\mathrm{d}\xi=\frac{\gamma'(t-m)^3}{3\cos^3\omega_i}(\sin\eta_i+\sin\omega_i). \tag{18}$$

By combining Eqs. (17) and (18), $f_{AB'}$ can be expressed as:

$$f_{AB'}=\frac{2(M_{II}+M_{III})}{|AB'|}=\frac{\gamma'(t-m)^2}{3\cos^2\omega_i}\left(2\sin\eta_i+2\sin\omega_i+\sin\eta_i\cos^2\eta_i\right). \tag{19}$$

Similarly, f_{AB} outside the caisson can be obtained as:

$$f_{AB}=\frac{\gamma' m^2}{3\cos^2\omega_o}\left(2\sin\eta_o+2\sin\omega_o+\sin\eta_o\cos^2\eta_o\right). \tag{20}$$

From Fig. 2, based on the force equilibrium of failure wedge I, the penetration resistance at the skirt-tip resulted from the self-weight of clay within plastic zones can be expressed as:

$$\sigma_{tip}=\frac{F_{tip}}{t}=\frac{f_{AB'}\cos\omega_i+f_{AB}\cos\omega_o-\gamma'\frac{t^2}{2}\sin\omega_i\sin\omega_o}{t}=\underbrace{\gamma'\frac{t}{2}\left[\left(1-\frac{m}{t}\right)^2\frac{4\sin\eta_i+4\sin\omega_i+2\sin\eta_i\cos^2\eta_i}{3\cos\omega_i}+\left(\frac{m}{t}\right)^2\frac{4\sin\eta_o+4\sin\omega_o+2\sin\eta_o\cos^2\eta_o}{3\cos\omega_o}-\sin\omega_i\sin\omega_o\right]}_{N_\gamma} \tag{21}$$

where, $m/t=\tan\omega_i/(\tan\omega_o+\tan\omega_i)$, ω_i, ω_o, η_i and η_o can be determined from Eqs. (1), (10) and (12), respectively. The bearing capacity factor N_γ has the value given in the square brackets of Eq. (21). Fig. 9b shows the values of factor N_γ versus adhesion factors, which range from 1.0 to 1.35 with respect to variations of the adhesion factors α_i and α_o.

As shown in Fig. 1, the geometry of the asymmetric failure mechanism can be defined by angles ω_i, ω_o, η_i and η_o that vary with adhesion factors α_i and α_o. For the smooth interface (i.e. $\alpha_i=\alpha_o=0$), the shear stress at the base of skit-tip $\tau_{tip}=0$, this gives $\omega_i=\omega_o=\eta_i=\eta_o=\pi/4$. As shown in Fig. 10a, the resulted failure mechanism coincides with that suggested by Meyerhof (1951). In this case, the corresponding bearing capacity factors N_c=8.28 and N_γ=1.

From Figs. 7 and 8, the radio shear zones II extend towards the skirt wall with the increasing skin friction, contributing to the penetration resistance of the skirt-tip. This coincides with the suggestion in Andersen et al. (2005) that N_c may be influenced by the skirt wall friction. Therefore, for the rough interface (i.e. $\alpha_i=\alpha_o=1$), the shear stress on the base of the skirt-tip $\tau_{tip}=s_u$ is potentially reached (i.e. the undrained shear strength of soil on the base of the skirt-tip is

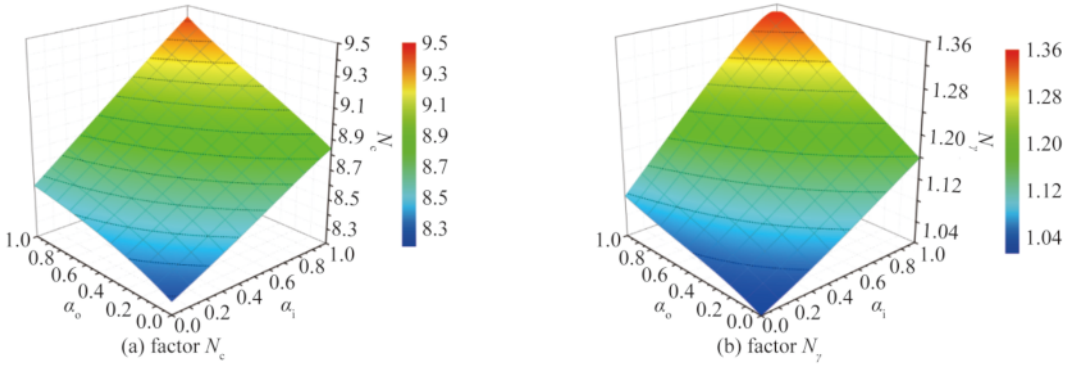

Fig. 9. Variations of bearing capacity factors with adhesion factors α_o and α_i.

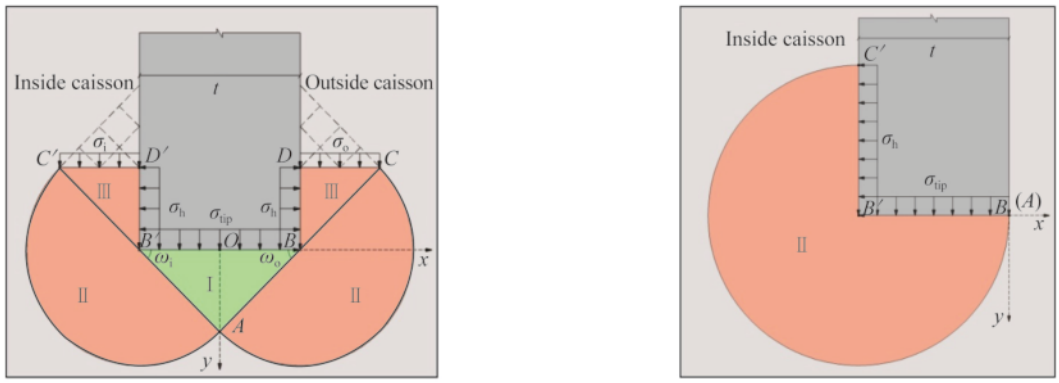

(a) Smooth interface (N_c=8.28, N_γ=1) (b) Rough interface (N_c=9.42, N_γ=1.35)

Fig. 10. Failure mechanism around the skirt-tip.

fully mobilized), giving ω_i=0, η_i=π/4 and ω_o=η_o=π/2. This leads to the failure wedge below the base of the skirt-tip vanishes and the radial shear zone II inside the caisson extends to the base of skit-tip BB' and inside of skirt wall $B'C'$ that have become β slip-lines as shown in Fig. 10b. In this case, the bearing capacity factors N_c=9.42 and N_γ=1.35. Overall, with the values of α_o and α_i being all between 0 and 1, the theoretical results of the factor N_γ range from 1.0 to 1.35, and factor N_c ranges from 8.28 to 9.42 that involves a typical value of about 9.0 usually assumed in design.

3 Calculation of required suction pressure, p_{re}

From Eq. (16), an important concern is to estimate the equivalent overburdens σ_i and σ_o at the skirt-tip level. As the caisson penetrates into seabed, the skin frictions along the skirt wall will enhance the vertical stresses in the vicinity of the skirt wall. As recommended by Houlsby and Byrne (2005), the downward adhesion will result in a uniform increase of vertical stress inside the caisson at the skirt-tip level. Then, the equivalent overburden σ_i inside the caisson at the skirt-tip level can be expressed as:

$$\sigma_i = \gamma' h + \frac{4h\alpha_i s_{u1}}{D_i} - p_{re}. \tag{22}$$

As suggested by Wu et al. (2020), the equivalent overburden σ_o at the skirt-tip level outside caisson will decrease exponentially with increasing distance from skirt wall. Thus, the maximum value of σ_o can be obtained at the skirt wall surface.

$$\sigma_o = \gamma' h + \frac{(1+1.5h/D)^2 \alpha_o s_{u1}}{1+3.5h/D}, \tag{23}$$

where, s_{u1} is the average shear strength over the penetration depth of skirt wall.

By combining Eqs. (1), (16), (21) (22) and (23), the penetration resistance of the skirt-tip σ_{tip} can be expressed in a standard form as:

$$\sigma_{tip} = N_q \sigma_z + N_c s_u + N_\gamma \gamma' \frac{t}{2}, \tag{24}$$

where, σ_z=($\sigma_i$tanω_o+$\sigma_o$tanω_i)/(tanω_o+ tanω_i); σ_i and σ_o can be obtained from Eqs. (22) and (23); ω_i and ω_o are calculated from Eq. (1); N_q=1 for undrained clay; N_c and N_γ can be determined from Eqs. (16) and (21) in terms of adhesion factor α_i and α_o. Nevertheless, if the skirt wall of caisson is painted or treated in other ways to reduce the skin friction, a correction factor needs to be applied to the calculation of skin friction between clay and skirt wall (Andersen et al., 2005; Guo et al., 2012). The correction factor can be determined from ring shear tests (Andersen et al., 2005). As discussed by Wu et al. (2020), the values of adhesion factors α_i and α_o may be different, which can be derived theoretically by using back analysis (House et al., 1999).

During suction-assisted penetration, the required suction pressure is calculated as the total penetration resistance (F_{tot}) minus the submerged caisson weight (V'), divided by the inside cross section area of the soil plug. Then, by using limit equilibrium theory of suction caisson in a vertical direction, the required suction pressure for caisson installation can be obtained as

$$p_{re} = \frac{F_i + F_o + F_{tip} - V_i}{\pi D_i^2/4} = \frac{\pi D h \alpha_o s_{u1} + \pi D_i h \alpha_i s_{u1} + \pi D_m t \sigma_{tip} - V'}{\pi D_i^2/4}, \tag{25}$$

where σ_{tip} can be determined from Eq. (24).

4 Verifications

4.1 Verification with FE calculation results

The geometry of the failure wedge is confirmed by the displacement contours and the moving pattern of soil below the smooth and rough bases of the skirt-tip obtained from finite (FE) element simulations. The detailed information about the FE calculations can be found in Wu et al. (2020). Fig. 11 shows the resulted displacement vectors and nephograms of soil below the skirt-tip at the penetration depth h/D=3.0.

It can be observed from Fig. 11a that a symmetrical failure wedge with base angles ω_i=ω_o=π/4 is formed below the smooth base where the soil moves downwards and inwards.

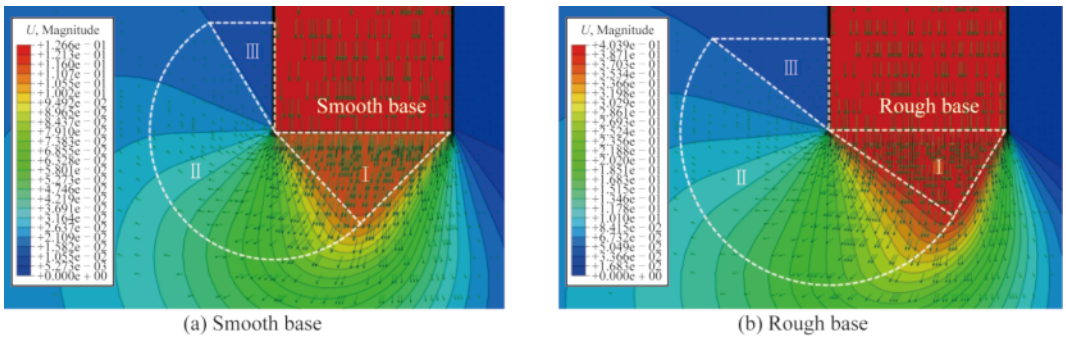

Fig. 11. Displacement vectors together with nephograms at penetration depth of h/D=3.0.

For a rough base, however, an asymmetric failure wedge formed below the base of the skirt-tip, which acts as part of the skirt wall, as shown in Fig. 11b. This reveals that the shear stress was induced at the rough base of the skirt-tip, restricting the horizontal movement of the failure wedge. Thus, it can be concluded from Fig. 11 that the base shear stress causes an asymmetrical geometry of the failure wedge below the base of the skirt-tip.

Since the difference in equivalent overburdens at the skirt-tip level between the outside and inside of the caisson increases with the increasing penetration depth h/D, the undrained shear stress of soil on the base of the skirt-tip will be gradually mobilized. At initial suction-assisted penetration depth h/D=1.5, the equivalent overburden σ_i is slightly larger than σ_o because the value of exerted suction inside the caisson (p_{re} = 4.5 kPa) is small. The degree of mobilization of shear strength of soil on the base of the skirt-tip is low on account of the little difference in equivalent overburdens at skirt-tip level between the inside and outside of the caisson, as shown in Fig. 12b. Thus, the apex A' of the failure wedge deviates the center line inward slightly, as shown in Fig. 12a.

However, as the skirt wall penetrates clay to a deeper position, the difference in equivalent overburdens between the outside and inside of the caisson at the skirt-tip level increases with the increasing exerted suction pressure. Therefore, the direction of shear stress on the base of the skirt-tip changes from inwards to outwards. Thus, the pole point moves from point a' to point a on a Morh circle, as shown in Fig. 12b. Meanwhile, the apex of failure wedge moves along arc $B'A'AB$ from point A' at h/D=1.5 to point A at h/D=4.0, as shown in Fig. 12a. This is confirmed by FE calculations as shown in Figs. 11 and 13, where the apex of the failure wedge deviates the center line of skirt wall from inward to outward with the increasing penetration depth, and finally remains almost unchanged until the end of suction-assistant penetration.

4.2 Verification with measured data and existing theoretical results

4.2.1 *Laboratory installation tests*

Three caissons with diameters of 10.4 mm, 15.9 mm and 37.2 mm were investigated by House et al. (1999) in normally consolidated clay. All caissons had a wall thickness of 0.4 mm and an L/D ratio of 8. The effective unit weight of the soil is 5.9 kN/m^3. In the centrifuge, the shear strengths of the normally consolidated clay are estimated to be 90 kPa/m for Sample I and 75 kPa/m for Sample II, respectively. Table 1 summarizes the optimal theoretical factors that provide the best fit to the experimental data of the caisson installations in House et al. (1999).

Fig. 14 shows comparisons between the calculated and measured results of required suction to install the caissons of 10.4 mm, 15.9 mm and 37.2 mm in diameter. It can be found that the predicted results from Eq. (25) with the values of adhesion factors α_i and α_i suggested in House et al. (1999) are in a good agreement with the measured data.

4.2.2 *Prototype tests*

Two caissons with diameters of 1.5 m and 3 m were in-

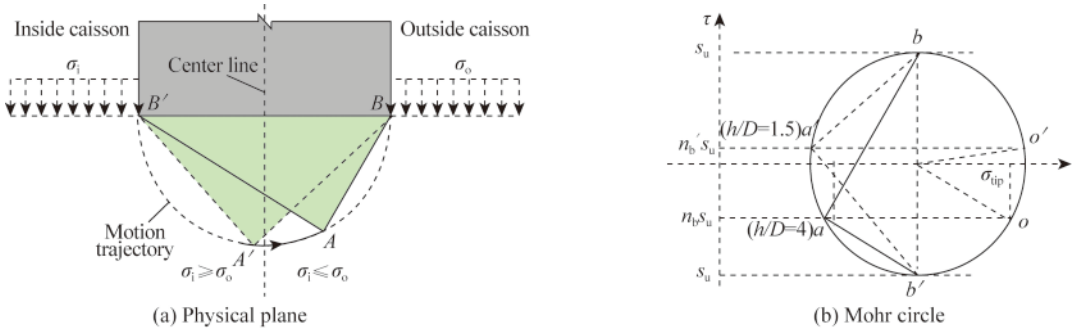

Fig. 12. Movements of apex of the failure wedge.

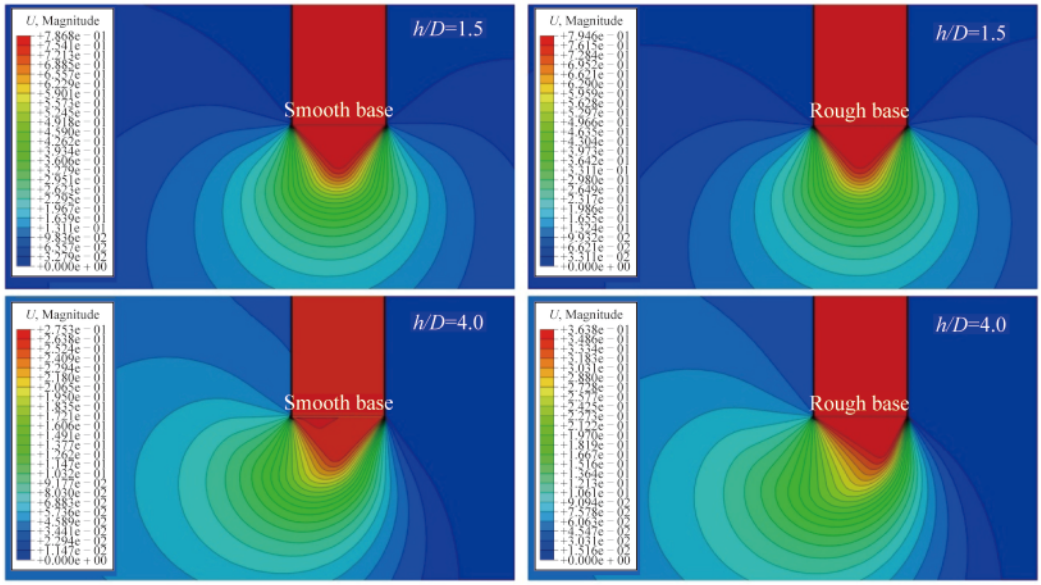

Fig. 13. Failure mechanisms at the penetration depths h/D=1.5 and 4.0.

Table 1 Values of adhesion factors recommended by House et al. (1999)

Clay		Sample I (ρ=90 kPa/m)		Sample II (ρ=75 kPa/m)		
Diameter (mm)		15.9	37.2	10.4	15.9	37.2
Factors	α_i	0.0	0.25	0.88	0.4	0.16
	α_o	0.75	0.75	0.7	0.6	0.62

vestigated in normally consolidated clay by Houlsby et al. (2005). The undrained shearing strength of the soil can be estimated as s_u=11.43+1.9z. As suggested by Houlsby et al. (2005), the adhesion factors α_i=α_o=0.5 were used for both the inside and outside of the skirt wall. More detailed information is available in Houlsby et al. (2005). Fig. 15 presents the comparison between the predicted results from Eq. (25) and the existing theoretical and test results in Houlsby et al. (2005).

Generally, the predictions of the required suction agree well with the measured data until the full penetration depth of the caisson is reached, except at the initial penetration depth. This may be due to the underestimated undrained shear strength of the shallow soil, leading to an underestimation of the required suction (Houlsby et al., 2005). Furthermore, the predicted theoretical result of the bearing capacity factor N_c=8.8 which is very close to N_c=9 that was adopted in Houlsby et al. (2005). The theoretical results of Eq. (25) for each caisson were in good agreement with existing theoretical results by adopting adhesion factors α_i and α_o suggested in Houlsby et al. (2005).

4.2.3 *Centrifuge model tests and FE simulation results*

House and Randolph (2001) conducted the centrifuge test to investigate the installation of suction caisson in normally consolidated clay. The experiments were carried out at 120 g. At the prototype scale, the strength profile of the clay increases with the depth at the gradient of 1.2 kPa/m from the mud-line to the depth of 8.04 m and then increases with the depth at the gradient of 1.7 kPa/m. The effective unit weight of the soil was 6.6 kN/m^3. The prototype geometry contrast with the model caisson is 3.6 m in diameter, 60 mm in wall thickness and 14.4 m in skirt length. An adhesion factor of 0.5 recommended by Houlsby and Byrne

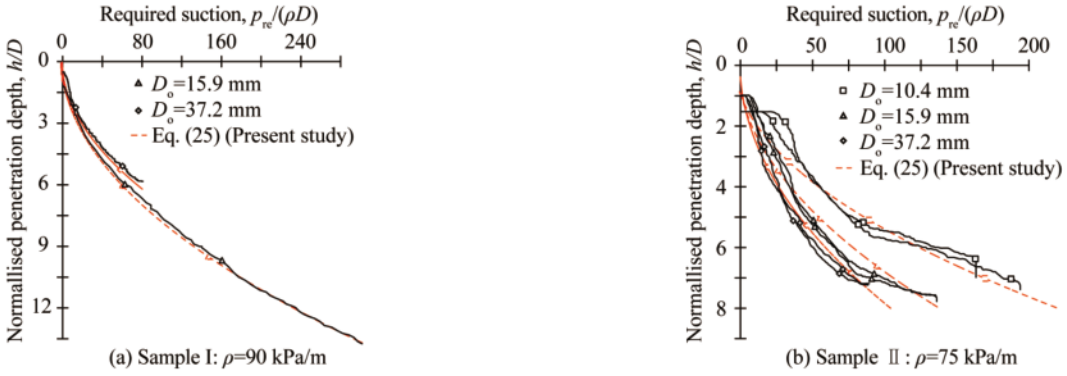

Fig. 14. Suction vs. penetration depth for model tests.

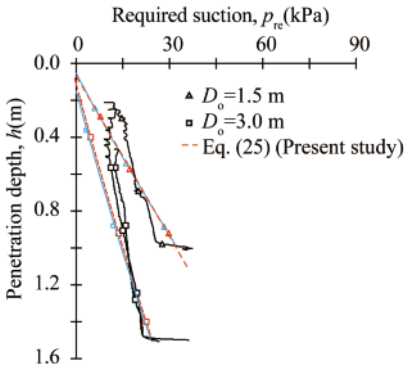

Fig. 15. Suction vs. penetration depth for prototype tests.

(2005) was used for both internal and external walls. Fig. 16 shows a comparison between the calculated and measured suction pressure. It can be observed that the theoretical results of Eq. (25) are in good agreement with that calculated in Houlsby and Byrne (2005) and the centrifuge test data. From Figs. 14−16, it can be seen that the required suction pressure predicted by Eq. (25) can present satisfactory comparisons with FE calculations, existing theoretical and experimental results.

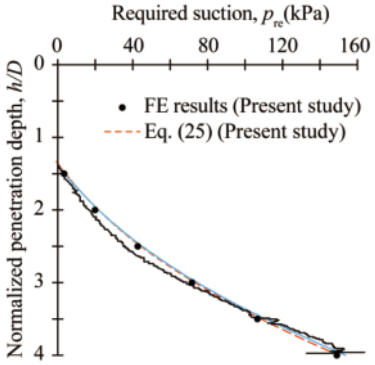

Fig. 16. Suction vs. penetration depth for centrifuge test.

5 Conclusions

With considering an asymmetry failure mechanism at the skirt-tip, the penetration resistance of skirt-tip for suction caisson penetrating in clay is deduced by using the slip-line method. The bearing capacity factors N_c and N_γ are expressed in terms of the adhesion factors α_i and α_o. The analytical solution to the required suction pressure to install suction caissons is obtained based on the force equilibrium in a vertical direction. By comparing with the FE calculation and experimental results, the proposed failure mechanism is validated and the predictions of the required suction pressure have been proved to be in good agreement with the measured data. The proposed method is helpful to understand the failure mechanism at the skirt-tip, and provides reliable results in selecting the bearing capacity factors N_c and N_γ to compute the skirt-tip resistance during suction-assisted penetration in clay. The following conclusions can be drawn.

(1) The shear stress τ_{tip} on the base of the skirt-tip leads to an asymmetrical geometry of the failure wedge. For a smooth base of the skirt-tip (i.e. τ_{tip}=0), a symmetry failure wedge is formed below the skirt-tip. For a rough base of the skirt-tip, the failure wedge below the base of the skirt-tip tilts outwards gradually with the increasing mobilized base shear stress τ_{tip}, and finally vanishes at the full mobilization of undrained shear strength (i.e. $\tau_{tip}=s_u$).

(2) The radio and passive plane shear zones identical to those of the failure mechanism for a deep foundation are formed at each side of the failure wedge. The radio shear zone extends towards the skirt wall with increasing adhesion factor, contributing to the skirt-tip resistance.

(3) The proposed failure mechanism considers the effect of adhesion factors on the failure mechanism at the skirt-tip, and involves the contribution from both the effective unit weight of soil and the weight average of equivalent overburdens at the skirt-tip level. For undrained clay, the resulted bearing capacity factors N_q=1, N_c and N_γ range from N_c=8.28 and N_γ=1 for smooth interface ($\alpha_i=\alpha_o$=0) to N_c=9.42 and N_γ=1.35 for rough interface ($\alpha_i=\alpha_o$=1).

References

Andersen, K.H. and Jostad, H.P., 1999. Foundation design of skirted foundations and anchors in clay, *Proceedings of the 31st Annual Offshore Technology Conference*, OTC, Houston, TX, pp. 383–392.

Andersen, K.H., Jostad, H.P. and Dyvik, R., 2008. Penetration resistance of offshore skirted foundations and anchors in dense sand, *Journal of Geotechnical and Geoenvironmental Engineering*, 134(1), 106–116.

Andersen, K.H., Murff, J.D., Randolph, M.F., Clukey, E.C., Erbirch, C.T., Jostad, H.P., Hansen, B., Aubeny, C., Sharma, P. and Supachawarote, C., 2005. Suction anchors for deepwater applications, *Proceedings of the International Symposium on Frontiers in Offshore Geotechnics* (*ISFOG*), Perth, Western Australia, pp. 3–30.

Byrne, W.B., Houlsby, G.T., Martin, C. and Fish, P., 2002. Suction caisson foundations for offshore wind turbines, *Wind Engineering*, 26(3), 145–155.

Chen, W. and Randolph, M., 2004. Radial stress changes around caissons installed in clay by jacking and by suction, *Proceedings of the 14th International Offshore and Polar Engineering Conference*, International Society of Offshore and Polar Engineers, Toulon, France, pp., 493–499.

Davis, E.H. and Booker J.R., 1973. The effect of increasing strength with depth on the bearing capacity of clays, *Géotechnique*, 23(4), 551–563.

Guo, Z., Wang, L.Z., Yuan, F. and Li, L.L., 2012. Model tests on installation techniques of suction caissons in a soft clay seabed, *Applied Ocean Research*, 34, 116–125.

Hossain, M.S., Lehane, B.M., Hu, Y. and Gao, Y., 2012. Soil flow mechanisms around and between stiffeners of caissons during installation in clay, *Canadian Geotechnical Journal*, 49(4), 442–459.

Houlsby, G.T. and Byrne, B.W., 2005. Design procedures for installation of suction caissons in clay and other materials, *Proceedings of the Institution of Civil Engineers-Geotechnical Engineering*, 158(2), 75–82.

Houlsby, G.T., Kelly, R.B., Huxtable, J. and Byrne, B.W., 2005. Field

trials of suction caissons in clay for offshore wind turbine foundations, *Géotechnique*, 55(4), 287–296.

House, A.R., Randolph, M.F. and Borbas, M.E., 1999. Limiting aspect ratio for suction caisson installation in clay, *Proceedings of the 9th International Offshore and Polar Engineering Conference*, International Society of Offshore and Polar Engineers, Brest, France, pp. 676–683.

House, A.R. and Randolph, M.F., 2001. Installation and pull-out capacity of stiffened suction caissons in cohesive sediments, *Proceedings 11th International Offshore and Polar Engineering Conference*, International Society of Offshore and Polar Engineers, Stavanger, Norway, pp. 574–580.

Li, D.Y., Guo, Y.X. and Gao, Y.F., 2013. Principle and application of pole point method of Mohr's circle, *Chinese Journal of Geotechnical Engineering*, 35(10), 1883–1888. (in Chinese)

Li, L.L., Dai. H.J. and Wang, L.Z., 2010. Behavior of installation for suction anchor in soft clay, *Proceedings of the ASME 2010 29th International Conference on Ocean*, *Offshore and Arctic Engineering*, ASME, Shanghai, China, pp. 823–829.

Luan, L.B., Ding, X.M., Zheng, C.J., Kouretzis, G. and Wu, Q., 2020. Dynamic response of pile groups subjected to horizontal loads, *Canadian Geotechnical Journal*, 57(4), 469–481.

Meyerhof, G.G., 1951. The ultimate bearing capacity of foundations, *Géotechnique*, 2(4), 301–332.

Meyerhof, G.G., 1955. Influence of roughness of base and ground-water conditions on the ultimate bearing capacity of foundations, *Géotechnique*, 5(3), 227–242.

Meyerhof, G.G., 1963. Some recent research on the bearing capacity of foundations, *Canadian Geotechnical Journal*, 1(1), 16–26.

Randolph, M., Cassidy, M., Gourvenec, S. and Erbrich, C., 2005. Challenges of offshore geotechnical engineering, *Proceedings of the 16th International Conference on Soil Mechanics and Geotechnical Engineering*, vol. 1, Osaka, Japan, pp., 123–176.

Randolph, M.F. and House, A.R., 2002. Analysis of suction caisson capacity in clay, *Proceedings of the Offshore Technology Conference*, OTC, Houston, Texas, pp. 2145–2155.

Randolph, M.F., O'Neill, M.P., Stewart, D.P. and Erbrich, C., 1998. Performance of suction anchors in fine-grained calcareous soils, *Proceedings of the Offshore Technology Conference*, OTC, Houston, Texas pp. 521–529.

Terzaghi, K., 1943. *Theoretical Soil Mechanics*, John Wiley and Sons, New York.

Watson, P.G., Randolph, M.F. and Bransby, M.F., 2000. Combined lateral and vertical loading of caisson foundations, *Proceedings of the Offshore Technology Conference*, OTC, Houston, Texas, pp. 797–808.

Westgate, Z.J., Tapper, L., Lehane, B.M. and Gaudin, C., 2009. Modelling the installation of stiffened caissons in overconsolidated clay, *Proceedings of the ASME 2009 28th International Conference on Ocean*, *Offshore and Arctic Engineering*, ASME, Honolulu, Hawaii, USA, pp. 119–126.

Wu, Y.Q., Li, D.Y., Zhang, Y.K. and Chen, F.Q., 2018. Determination of maximum penetration depth of suction caissons in sand, *KSCE Journal of Civil Engineering*, 22(8), 2776–2783.

Wu, Y.Q., Wang, Z.T., Yang, Q. and Li, D.Y., 2019. Theoretical studies on penetration resistance of suction caissons in clay, *Marine Georesources and Geotechnology*, 37(5), 558–567.

Wu, Y.Q., Zhang, Y. and Li, D.Y., 2020. Solution to critical suction pressure of penetrating suction caissons into clay using limit analysis, *Applied Ocean Research*, 101, 102264.

Zhang, P.Y., Guo, Y.H., Liu, Y.G. and Ding, H.Y., 2016. Experimental study on installation of hybrid bucket foundations for offshore wind turbines in silty clay, *Ocean Engineering*, 114, 87–100.

Zhou, H.J. and Randolph, M.F., 2006. Large deformation analysis of suction caisson installation in clay, *Canadian Geotechnical Journal*, 43(12), 1344–1357.